A Comparison of Six Transport Models of the MADE-1 Experiment implemented with Different Types of Hydraulic Data

Alraune Zech[1,2], Sabine Attinger[2,3], Alberto Bellin[4], Vladimir Cvetkovic[5], Gedeon Dagan[6], Marco Dentz[7], Peter Dietrich[2,8], Aldo Fiori[9], Georg Teutsch[2]

[1]Department of Earth Science, Utrecht University, The Netherlands
[2]Helmholtz Centre for Environmental Research - UFZ, Leipzig, Germany
[3]Institute of Earth and Environmental Science-Geoecology, University Potsdam, Germany
[4]Department of Civil, Environmental and Mechanical Engineering, University of Trento, Italy
[5]Department of Water Resources Engineering, Royal Institute of Technology, Stockholm, Sweden
[6]School of Mechanical Engineering, Tel Aviv University, Ramat Aviv, Israel
[7]Institute of Environmental Assessment and Water Research (IDAEA), Spanish National Research Council, Barcelona, Spain
[8]Center of Applied Geoscience, University of Tübingen, Tübingen, Germany
[9]Department of Engineering, Roma Tre University, Rome, Italy

Key Points:

- Predictions of transport in highly heterogeneous aquifer are achieved with six models of different conceptualization and field data input
- Models' predictions are reliable if they share similar values of mean velocity and permeability degree of variability and correlation scale
- The MADE site plume longitudinal mass distribution is a robust transport measure

Corresponding author: Alraune Zech, a.zech@uu.nl

Abstract

Six conceptually different models of steady groundwater flow and conservative transport are applied to the heterogeneous MADE aquifer. Their predictive capability is assessed by comparing the modelled and observed longitudinal mass distributions at different times of the plume in the MADE-1 experiment, as well as at a later time. The models differ in their conceptualization of the heterogeneous aquifer structure, computational complexity, and use of permeability data obtained from various observation methods (DPIL, Grain Size Analysis, Pumping Tests and Flowmeter). Models depend solely on aquifer structural and flow data, without calibration by transport observations. Comparison of model results by various measures, i.e. peak location, bulk mass and leading tail, reveals that the predictions of the solute plume agree reasonably well with observations if the models are underlined by a few parameters of close values: mean velocity, a parameter reflecting log-conductivity variability and a horizontal length scale related to conductivity spatial correlation. From practitioners perspective the robustness of the models is an important and useful property. The model comparison provides insight into relevant features of transport in heterogeneous aquifers. After further validation by additional field experiments or by numerical simulations, the results can be used to provide guidelines for users in selecting conceptual aquifer models, characterization strategies, quantitative models and implementation for particular goals.

1 Introduction

Modelling contaminant transport by groundwater is a topic of great interest that stimulated intensive research in the last four decades due to its relevance to aquifer pollution (Dagan, 1989; Gelhar, 1993; Fetter et al., 2018). The task of predicting transport faces a few difficulties: the processes are of long duration, measurements are scarce, the subsurface medium is of complex heterogeneous structure subjected to uncertainty and many times the geometry and the mass content of the contaminant source is also not known with certainty.

Under these circumstances models play an important role: they help understanding the involved processes, analysing field data and making long range prediction. Models developed in the past differ in conceptualization of the aquifer structure, in the required data, in quantification of transport, in the formulation of the governing equations and mechanisms they represent, in computational complexity and in models goals.

We focus on transport of plumes of conservative solutes in steady natural gradient flow, driven by a constant mean head gradient. Quantification of the spatial distribution is by $m(x,t)$, mass per unit length, where x is the mean flow direction and t the time. It encapsulates the process of longitudinal spreading in space and time. In practice it allows, for instance, to estimate the mass of solute pumped by wells or flowing into rivers or reservoirs. It also serves as a first step toward achieving other goals like determining the local concentration $C(\mathbf{x},t)$.

There is general agreement that spatial variability of the hydraulic conductivity $K(\mathbf{x})$ is the main growth mechanism responsible for plume spreading in aquifers, termed macrodispersion (Zech et al., 2015). The effect increases with higher K heterogeneity as quantified for instance by the log-conductivity variance σ_Y^2.

A few elaborate field experiments were conducted in the past in order to gain understanding and validate models. The most challenging one is at the *MADE* site (Boggs et al., 1992), situated in a highly heterogeneous aquifer, making it of relevance to many actual aquifers (Gomez-Hernandez et al., 2017). An important feature of *MADE* was the application of different observation methods in order to characterize the K spatial distribution (e.g. Boggs et al. (1990); Rehfeldt et al. (1992); Bohling et al. (2016)). Long-term tracer tests provide graphs of observed mass distribution $m(x,t)$ in space at a few

fixed t values (Boggs et al., 1990, 1995). It has motivated a flurry of works on structure characterization by field data and different modelling strategies (see e.g. Zheng et al. (2011)). We will elaborate on *MADE* in section 2.

We examine the ability of six conceptually different models to predict the observed mass m. Subsequently, we examine the predictive power of the models by extending the time ($t = 1000$ days) beyond *MADE* observations ($t_{\max} = 503$ days). The selected models, outlined in Section 3, differ in conceptualizations of formation structure and transport, in the use of field data, in initial conditions, in computational methodology and in effort. A few of the models were developed in the past while the others were formulated for use in the present paper. The models cover a wide spectrum of configurations. We concentrate here only on models that can predict transport based on field data of aquifer properties and flow; we do not consider models calibrated on prolonged transport tests which are generally of large duration and cost.

We believe that the comparison of the models which differ in type and underlying field data, conceptualization of K spatial structure and complexity of computations by using *MADE* as a platform is important in helping the research community to grasp transport issues and the users in selecting characterization strategies, goals of models and method implementation.

The plan of the paper is as follows: Sect. 2 recapitulates the *MADE* aquifer characterization and transport experiment; Sect. 3 describes the methodology of the models, including their application to *MADE*; Sect. 4 is devoted to the model prediction for solute mass m in comparison to *MADE* observations as well as time beyond. Sect. 5 contains the general discussion on data comparison while Sect. 6 concludes the paper.

2 MADE Transport Field Experiment

The *MADE* experiment was the object of a large body of publications dealing with the aquifer properties data collection and analysis as well as transport observations and interpretation (see for instance reviews Zheng et al. (2011); Gomez-Hernandez et al. (2017)). We recall in the following only those aspects of *direct* relevance to the examined models.

2.1 Hydraulic Conductivity Spatial Distribution

The MADE site aquifer is composed of highly heterogeneous alluvial terrace deposits. Measurements of hydraulic conductivity at multiple locations (see Fig. 1) were performed by granulometry of soil samples, flow meter, slug test, and Direct Push Injection Logger (DPIL) (Boggs et al., 1990; Rehfeldt et al., 1992; Bohling et al., 2016). Besides, two pumping tests provide equivalent conductivities K_{eq} of the volume surrounding the wells (Boggs et al., 1992). The use of different techniques at same site and subsequent application by different models offers an unique opportunity to examine their impact on transport prediction.

The spatially distributed observations (Fig. 1), carried out at different depths resulted in a large volume of data which served for geostatistical analysis. Fig. 2 summarizes their outcomes, which is of interest for the application of the different models (Sect. 3). The most reliable and extensively used data are those based on flowmeter (Boggs et al., 1990; Rehfeldt et al., 1989) with a total number of $N = 2611$ observations and more recently DPIL with $N = 31123$ (Bohling et al., 2012, 2016).

The differences in the geostatistical parameters, especially in the geometric mean K_{G}, are a result of the different properties of the observation methods as well as the density and locations of observation points. Particularly, the difference between flowmeter and DPIL can be explained by the inability of flowmeter to detect low K values. While

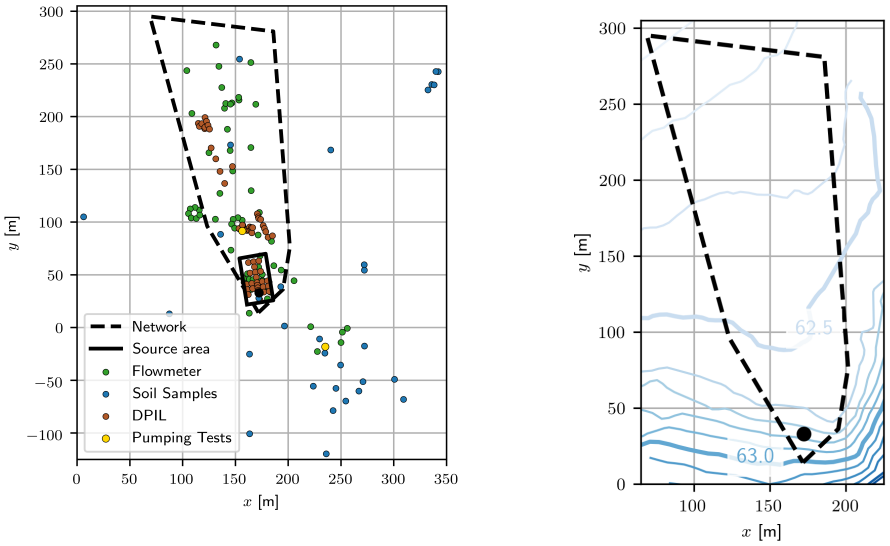

Figure 1. Left: Map of MADE site according to Boggs et al. (1990); Bohling et al. (2016): Locations of hydraulic conductivity measurements devices (coloured dots); tracer test source area (black outline); and sampling network boundary (dashed outline) where bromide samples were collected. Right: Potentiometric surface map of head measurements according to Boggs et al. (1990). Black dot marks tracer test injection location.

the maximal values $K_{\max}$ are close (around 0.005 m/s) the minimal values $K_{\min}$ differ by two orders of magnitude. The effect manifested in Fig. 2 is that flowmeter K_{G} is larger and σ^2_{Y} is smaller. The difference in the longitudinal integral scales I_h suggests that the zones of low K values are less connected than those of higher magnitude. The analysis based on soil samples ($N = 214$) is less reliable. Still, it provided input data for conductivity conceptualization based on the lithofacies approach (e.g. Carle & Fogg (1996)) as presented by Bianchi & Zheng (2016) and herein for a simplified binary structure approach. The impact of these difference upon flow and transport are discussed in Sect. 4.

2.2 Flow

In Fig. 1 we reproduce the head contour lines map (Boggs et al., 1992, Fig. 3). The head gradient is not constant, but slowly varying in space. The mean head gradient is between $J \in [0.003, 0.0036]$ depending on the choice of boundary locations. The non-uniformity of the head contour density indicates the presence of large scale mean hydraulic conductivity trends.

2.3 Transport Experiment

We focus on the first tracer transport experiment, which was conducted in years 1986–1988 (Boggs et al., 1990, 1992; Rehfeldt et al., 1992; Adams & Gelhar, 1992). The tracer plume displayed a non-Gaussian longitudinal solute mass distribution with the bulk of the mass staying near the source, but with lower amounts spreading downgradient extensively.

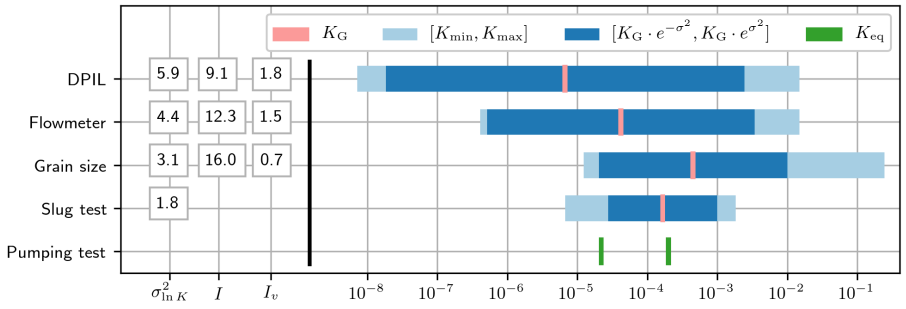

Figure 2. Geostatistical measures for MADE from DPIL (direct push injection logging) (Bohling et al., 2016), flowmeter, grain size analysis, slug tests (Rehfeldt et al., 1992): log-conductivity variance $\sigma^2_{\ln K}$, horizontal and vertical integral scale (correlation length) I and I_v, respectively. Visualization of geometric mean conductivity K_G, range of observed values from minimal to maximal ($[K_{min}, K_{max}]$), and range of one variance around mean ($[K_G \cdot e^{-\sigma^2}, K_G \cdot e^{\sigma^2}]$). K_{eq} denotes the equivalent conductivity for two large scale pumping tests (Boggs et al., 1990).

Initial Conditions: A quantity of $M_0 \cong 25$ kg of Bromide dissolved in 10 m^3 of water was injected over a period of 48 hours through 5 wells of half a meter screen length. While the subsequent transport took place under practically mean uniform flow conditions, the tracer solution was forced radially into the aquifer during injection. As a result, the initial tracer body was much larger than the body adjacent to the wells screens, which can be seen in the early tracer plume snapshot at 9 days after injection (Adams & Gelhar, 1992, Fig.5). This is important as far as ergodicity and setup of initial conditions are concerned. The apparent upstream tracer spread cannot be interpreted as a result of upstream dispersion. The injection mode also implies that the initial condition was flux proportional, with a preference of mass flowing in high conductivity channels.

Plume Detection and Data Aggregation (Upscaling): We reproduce the longitudinal mass distribution $\bar{m}(x,t)$ of Adams & Gelhar (1992, Fig.7) at six times T: 49, 126, 202, 279, 370, and 503 days after beginning of injection. The computation of $\bar{m}$ is based on concentration $C(x,y,z,t)$ sampled in a dense MLS network, which thins out with distance to the source (Fig. 1). Subsequently, C was numerically integrated over transverse planes (y,z), accumulated and averaged over slices of 10 m length in the x direction to obtain the upscaled longitudinal mass $\bar{m}(x,t)$ (Adams & Gelhar, 1992). The reported mass is displayed at the centers of the slices at $x = -5$ m, 5 m, 15 m, ... (see discussion of difference between the fine scale m and the upscaled one $\bar{m}$ in the sequel).

The fact that the reported mass is an upscaled/aggregated quantity, was overlooked by many previous studies which compared $\bar{m}$ with modeled mass at fine scale, as mentioned by Fiori et al. (2019). The significance of data aggregation is discussed in section 4 herein.

Mass Recovery The reported mass $\bar{m}$ does not obey the mass conservation requirement $\int \bar{m}(x,t)\, dx = 1$ except at 126 days after injection. Mass apparently decreases over time after 126 days with recovery rates of 2.06, 0.99, 0.68, 0.62, 0.54, and 0.43, for the $T = 49$, 126, 202, 279, 370, and 503 days, respectively.

As discussed in Adams & Gelhar (1992), the excessive mass recovery at $t = 49$ days could be due to spurious hydraulic connections among the multilevel samplers. This is a result of the method of installation and is enhanced by the pressure of injection. Pref-

erential sampling from high conductivity regions is also possible. In such case, the assumption of uniform tracer distribution employed in the spatial integration easily leads to an overestimated mass recovery.

We attribute the apparent mass loss at later times to insufficient sampling in the downstream zone in line with Fiori (2014). The high heterogeneity implies possible channeling effects at *MADE*. In combination with the much lower sampling density downstream, it is generally difficult to sample the leading edge of the plume, which may contain a significant fraction of the plume mass (Fiori et al., 2019).

Unlike some authors, we do not normalize observed mass $\bar{m}$ by the total reported mass i.e. $\tilde{m} = \bar{m}(x,t)/\int \bar{m}(x,t)\,dx$, but use $\bar{m}$ for comparison with theoretical models, as it is appropriate for a conservative solute. Normalizing would imply that mass apparent loss is proportional to the observed mass.

3 Subsurface Transport Models

3.1 Common Features and Prerequisites

We compare various models which were developed independently by the authors in the past or devised recently in the frame of the present study. Before describing the models specific properties, we recapitulate a few common features:

1. We examine only predictive models. They rely solely on structural and flow data which can be measured independently of transport. Models with parameters calibrated by transport experiments are not considered.
2. Flow is steady and uniform in the mean (natural gradient), driven by the steady head gradient J in the x direction.
3. Transport is advective and spreading is caused by the spatial variability of $K(\mathbf{x})$. The effective porosity θ is assumed to be constant.
4. A plume of mass M_0 of a conservative solute is injected initially in the aquifer at $t = 0$. Spreading is quantified by the mass arrival at a control plane at x: $M_{total}(x,t) = \theta \int_x^\infty \int\int C(x',y,z,t)dx'dydz$, where C is the concentration. For a fixed x, $M = M_{total}\ /M_0$ is the BTC whereas for a fixed t it is the relative mass accumulated beyond x.
5. We determine the fine scale relative mass spatial distribution $m(x,t) = -\partial M/\partial x$ at a few times t. However, in line with *MADE* observations, we calculate the (upscaled) relative mass averaged over a medium slice of length $\Delta = 10\,\mathrm{m}$ centered at x, which is given by $\bar{m}(x,t;\Delta) = (1/\Delta)[M(x-\Delta/2,t) - M(x+\Delta/2,t)]$ such that $m = \lim_{\Delta \ll I} \bar{m}$.
6. The upscaled relative mass $\bar{m}$ is derived for the *MADE* conditions at t =49, 126, 202, 279, 370, and 503 days after injection toward comparison with measured $\bar{m}$. Additionally, models are applied to prediction of $\bar{m}$ at $t = 1000$ days for intercomparison. As useful additional quantification we also consider the mass flux through the control plane, $\mu(x,t) = \partial M/\partial t$.

Remark on additional MADE transport Models: Several other transport models which are not discussed here have been presented in the literature for *MADE*. We do not consider models calibrated on transport observations since they are not predictive, such as the work of Barlebo et al. (2004). This further includes dual-domain models (e.g. Harvey & Gorelick (2000) and Feehley et al. (2000)) and the continuous time random walk (CTRW) model of Berkowitz & Scher (2001). The lithofacies approach of Bianchi & Zheng (2016) would have been a candidate but results are only available for the *MADE*-2 tracer experiment setting rather than *MADE*-1 considered here. The same holds for the work of Salamon et al. (2007). The conceptual framework is however underlying the facies model herein. Similarly, the fractional ADE model of Benson et al. (2001) is applied only to

MADE-2 data. Furthermore, not all parameters, such as the skewness parameter β, are fully predictive based on structural data only. Dogan et al. (2014) presented a predictive fully numerical transport model for the *MADE*-1 experiment based on flowmeter and DPIL measurements. They generated detailed representations of the K field conditioned to observations in a small sector of the *MADE* site aquifer and subsequently solved the flow and transport equations. However, due to the computational effort, transport simulation results are limited to a fraction of the total plume transport distance. Thus, their results are unsuitable for model comparison, particularly with prediction beyond observation times.

3.2 Brief Description

3.2.1 First Order Approximation (FOA)

Background The solution of flow and transport in heterogeneous formations of a random $Y = \ln K$ structure by a first order approximation in the log-conductivity variance σ_Y^2 was the topic of intensive research in the last four decades (see e.g. the monographs Dagan (1989); Gelhar (1993); Rubin (2003)) leading to various analytical solutions. We briefly recall past results and recent advances relevant to this work.

K-Structure The random Y field is regarded as stationary and multi-Gaussian. It is characterized completely by K_G, σ_Y^2, and the two point covariance C_Y of horizontal integral scale I and vertical one I_v. The anisotropy ratio $e = I_v/I$ is generally smaller than unity.

Flow The mean velocity is given by $U = K_{\text{eff}}J/\theta$, with the effective conductivity $K_{\text{eff}}/K_G = \text{func}(\sigma_Y^2, e)$ determined from the solution of the flow equations for the random velocity field. The latter is obtained by expanding the mass conservation equation and Darcy's law in power series in $Y' = Y - \langle Y \rangle$.

Transport Traditionally, the mean relative mass distribution $\langle m(x,t) \rangle$ was derived for conditions of given initial deterministic resident concentrations $C_0(\mathbf{x}, 0)$ either in a volume V_0, with $C_0 = M_0/(\theta V_0)$, or with mass concentrated on the plane $x = 0$ over an area A_0 and quantified by $m_0 = M_0/A_0$ (Kreft & Zuber, 1978). Similarly, detection was in the resident mode with the mean $\langle M \rangle$ and $\langle m \rangle$ satisfying the ADE

$$\frac{\partial \langle M \rangle}{\partial t} + U \frac{\partial \langle M \rangle}{\partial x} = D_L(t) \frac{\partial^2 \langle M \rangle}{\partial x^2} \tag{1}$$

The macrodispersion coefficient $D_L = U\alpha_L$, with longitudinal macrodispersivity α_L, was determined in the Lagrangean framework with the aid of the solute particles trajectories. At first order $\alpha_L(t)$ grows from zero at $t = 0$ to an asymptotic constant value $\alpha_L = \sigma_Y^2 I$ (Dagan, 1989). The transient $\alpha_L(t)$ was determined by a quadrature for an exponential covariance and is approximated accurately by an analytical expression as function of mean flow velocity, time and aquifer statistics: $\alpha_L(t)/\sigma_Y^2 I = \text{func}(Ut/I, e)$ (Dagan & Cvetkovic, 1993, Eq. 20). The asymptotic value is attained after a travel distance of a few integral scales I. The Gaussian solution approximates $\langle m \rangle$ satisfactorily for field experiments in weakly heterogeneous aquifers like Cape Cod (Hess et al., 1992) and Borden Site (Sudicky, 1986) and/or far from the injection zone. However, it failed to model the highly skewed mass distribution observed at *MADE* close to the injection zone. This finding has motivated development of new nonlinear models.

Fiori et al. (2017) presented the solution of the ADE (1) for the more realistic conditions of flux proportional injection. The solution for the BTC is given by the inverse Gaussian distribution:

$$\langle M \rangle = \frac{1}{2} \left\{ \text{erfc}\left(\frac{x - Ut}{2\sqrt{D_L t}} \right) + \exp\left(\frac{Ux}{D_L} \right) \text{erfc}\left(\frac{x + Ut}{2\sqrt{D_L t}} \right) \right\} \tag{2}$$

Unlike the Gaussian solution of Eq. (1), $\langle m(x,t)\rangle = -\partial\langle M\rangle/\partial x$ from Eq. (2) displays a skewed shape and lack of upstream dispersion. Jankovic et al. (2017) showed that the solution (2) with dispersion by first-order approximation $D_L(x)$ represents accurately the results of numerical simulations even for the large value of $\sigma_Y^2 = 8$ except an underestimation of a few percents of the mass in the tail of late arrival. We apply Eq. (2) to predict the *MADE* plume in the sequel as part of models comparison.

Application to MADE Application of Eq. (1) to *MADE* was based on the parameters derived from Bohling et al. (2016) by DPIL as follows: $K_{\rm G} = 0.58m/d$, $\theta = 0.31$, $I = 9.1m$, $I_v = 1.8m$, $\sigma_Y^2 = 5.9$. Rather than the first order approximation we used the more general formula by Zarlenga et al. (2018, Eq. 5) to arrive at $K_{\rm eff} = 2.28\,{\rm m/d}$. After identifying the representative mean head gradient in the plume zone (Fig. 1) as $J = 0.0036$, the mean velocity is given by $U = K_{\rm eff}J/\theta = 0.026\,{\rm m/d}$. Subsequently, the transient regime is taken into account by using a preasymptotic Dispersion $D_{\rm L}(x)$ $=U\alpha_{\rm L}(x)$, calculated according to Fiori et al. (2019, Eqs. C1,C2) based on $\alpha_{\rm L}$ of (Dagan & Cvetkovic, 1993, Eq. 20), with the asymptotic value $\alpha_{\rm L} = \sigma_Y^2 I = 53.7m$. This was the information needed in order to derive $\langle\bar{m}\rangle$ based on Eq. (1) at the t and x values pertinent to *MADE*.

3.2.2 Multi-indicator Model and Self Consistent Approximation (MIMSCA)

Background *MIMSCA* was developed in the last 15 years as an approximate model of flow and transport for aquifers of arbitrary degree of heterogeneity (Dagan & Fiori, 2003; Fiori et al., 2006; Cvetkovic et al., 2014). Its outcome has been compared with accurate numerical solutions for $\sigma_Y^2 \leq 8$ and applied to *MADE*. Fiori et al. (2019) recently applied the model to assess the uncertainty of prediction due to non-ergodic conditions or parametric uncertainty.

K - Structure The aquifer is modeled as an ensemble of rectangular inclusions tessellating the space similarly to layers of bricks. The elements are of dimension $2I\times$ $2I \times 2I_v$. The block K values are assigned independently with random values from a univariate pdf $f(K)$ (multi-indicator model). As usual, $f(K)$ was chosen to be lognormal of parameters K_G, σ_Y^2. This way the random K field is completely defined in terms of 4 parameters, similarly to the *FOA* (section 3.2.1).

Flow The mean velocity is given by $U = K_{\rm eff}J/\theta$. The mean effective conductivity $K_{\rm eff}$ is derived by the self consistent approximation *(SCA)*, a well established method in the literature on heterogeneous aquifers (Dagan, 1989). Here, it consists in solving the flow equations for a generic inclusion of conductivity K, submerged in a homogeneous matrix of the unknown $K_{\rm eff}$ and determining the latter by the *SCA* argument. $K_{\rm eff}$ follows as solution of a simple integral equation. Suribhatla et al. (2011) compared it with accurate numerical simulations with satisfactory agreement.

Transport Transport for the *MIM* was solved also with the *SCA*. Fiori et al. (2003) determined analytically the travel time required for a solute particle to move over an inclusions of conductivity K, surrounded by a matrix of K_{eff}. The BTC $\langle M\rangle$ follows as sum over the travel time random residuals pertaining to the inclusions of different K lying between the injection plane $x = 0$ and the control plane at x and the initial condition was of flux proportional injection at $x = 0$ while the mean BTC was derived by fast Fourier transform. Jankovic et al. (2003) showed a satisfactory agreement between the semi-analytical results and accurate 3D numerical simulations. Fiori et al. (2017) showed that the bulk of the BTC is well approximated by the *FOA*, while *MIMSCA* captures also the long tail of a few percents of the solute mass observed in numerical simulations.

Application to MADE Fiori et al. (2013) applied the method to the *MADE* site transport setting for $\langle m \rangle$ and for $\langle \bar{m} \rangle$, with an update in Fiori et al. (2019) motivated by an update in geostatistical input parameters by Bohling et al. (2016). The needed parameters values are the same as those given above for *FOA*.

3.2.3 TDRW

Background Time-domain random walk and continuous time random walk approaches have been used extensively over the past two decades for the modeling of transport in heterogeneous porous media (Noetinger et al., 2016). Within this framework and based on the stochastic TDRW method of Comolli et al. (2019), Dentz et al. (2020) derived a predictive upscaled model that avoids calibration by transport observations. The basic idea is to quantify particle motion in spatially variable flow fields through a Markov processes for equidistant particle velocities, whose steady state distribution is given by the flux-weighted distribution of flow velocities. While details can be found in Dentz et al. (2020), we describe here the main features of the model. This modeling approach has been used and verified for the prediction of the evolution of particle velocity statistics, particle distributions, dispersion and breakthrough curves in pore and Darcy scale heterogeneous porous media (Hakoun et al., 2019; Comolli et al., 2019).

K-Structure Hydraulic conductivity is represented by a three-dimensional log-normally distributed multi-Gaussian spatial random field. Thus, the random K-field is characterized in terms of 4 parameters, similarly to the *FOA* (section 3.2.1): geometric mean conductivity K_{G}, $\ln K$ variance, and correlation lengths ℓ_h and ℓ_v. Random realizations were filtered such that the spatial mean and variance of the log hydraulic conductivity are within a 5% tolerance interval around the target values.

Flow Model Groundwater flow is the result of the steady state groundwater flow equation, which is solved numerically on multi-Gaussian hydraulic conductivity fields characterized by a log-normal marginal distribution. A unit head drop between inlet and outlet is considered and no-flux boundaries are specified at the horizontal domain boundaries. The target variable is the magnitude of the Eulerian velocity $v_e(\mathbf{x})$ (absolute value of the Eulerian velocity), which is characterized by a uni-variate distribution. It is obtained from the numerically obtained magnitude of the Darcy velocity $q(\mathbf{x})$ by multiplication with the magnitude J of the head gradient, and geometric mean conductivity K_{G}, and division by (constant) porosity θ, thus $v_e(\mathbf{x}) = q(\mathbf{x})K_G J/\theta$.

Transport Model Transport is modeled by a continuous time random walk. Thus, particles move at constant space increment at transition times that are obtained from the particle velocity. The plume mass distribution at a given time is equivalent to the particle distribution. The particle velocity is modeled as a stationary Markov process, whose steady state distribution $p_v(v)$ is given by the flux-weighted Eulerian flow velocity. The flux-weighting is due to the fact that in this framework particle velocities sample the flow velocity equidistantly along path lines. This is in contrast to isochrone sampling in classical Lagrangian frameworks, for which the steady state distribution of particle velocities is equal to the Eulerian velocity distribution (Dentz et al., 2016; Comolli et al., 2019).

The Markov process of particle velocities is modeled through an Ornstein-Uhlenbeck process for the normal scores. The normal scores are obtained by mapping the velocities first to a uniform and then to a unit Gaussian random variable. The model requires the Eulerian velocity distribution and advective tortuosity as inputs. The latter is given by the ratio of the mean Eulerian velocity and the mean Eulerian velocity component along the mean hydraulic gradient.

Application to MADE For application to MADE, the model is parameterized based on the description of experimental conditions and aquifer properties as head gradient of $J = 0.0036$ and porosity of 0.31 according to Boggs et al. (1992); Adams & Gelhar (1992). The retardation coefficient is set equal to one. The distribution of Eulerian velocity magnitude as the propagator of the upscaled transport model is derived using the geostatistical parameters of log-normal hydraulic conductivity reported by Bohling et al. (2016) (Fig. 2). The average velocity component in mean flow direction is given by $\overline{v}_1 = \overline{q}_1 K_G J/\theta = 1.942\times10^{-7}$ m/s $= 0.0167$ m/d. The average Eulerian velocity magnitude is $\overline{v}_e = \overline{q} K_G J/\theta = 2.234$ m/s $= 0.0193$ m/d.

A point source particle distribution is assumed. Following Boggs et al. (1992) and Fiori et al. (2013), the initial mass distribution is approximately flux-weighted. Thus, in this modeling framework, the initial distribution of particle velocities is set equal to the flux-weighted Eulerian velocity distribution (Dentz et al., 2020).

3.2.4 Binary Facies

Background An alternative approach to adopting continuous univariate Y distribution consists in representing the media as an assemblage of hydrofacies. Among the geostatistical methodologies adopted for this purpose, the one based on the combined use of transition probability and Markov chain has been mostly employed since its introduction by Carle & Fogg (1996). It enjoys flexibility in handling justapositonal tendencies among hydrofacies and the availability of the software T-PROGS (Carle, 1999). In the context of the studies of *MADE*, Bianchi & Zheng (2016) presented an application to the *MADE-2* experiment by adopting representation by 5 hydrofacies. Here we apply the methodology to the *MADE-1* experiment in a more parsimonious way. We maintain the highly conductive hydrofacies and combine the remaining four, of low conductivity, into a single hydrofacies.

K-Structure The porous media is modeled by using two or more facies, each one of constant hydraulic conductivity. The spatial distribution of the facies is generated randomly based on transition probabilities, e.g. by using T-PROGS. Hydrofacies indentification is usually based on granulometry analysis. Here we focus on two hydrofacies of probabilities of occurrence p_1 and p_2, respectively. Hydraulic conductivities $K_{1,2}$ are the weighted arithmetic means of the hydraulic conductivity of all samples belonging to the same granulometry class, i.e. hydrofacies. The hydraulic conductivity of the samples are calculated from the characteristic diameters d_{10} and d_{25} of the sediments by using a modified version of the Kózeni-Carman expression proposed by Riva et al. (2010). Transition probabilities between hydrofacies are obtained by fitting a Markov model to the experimental transition probabilities (Carle & Fogg, 1996). They are expressed with the aid of the characteristic thickness and length for each facies, denoted as $L_{z,1}$, $L_{z,2}$, $L_{x,1}$, and $L_{x,2}$ respectively. Commonly, samples density is relatively low in the horizontal directions, leading to uncertain experimental transition probabilities in these directions, even after assuming isotropy in the horizontal plane.

Flow and Transport Flow and transport are solved repetitively in a Monte Carlo frame by making use of numerical solvers, Modflow 2005 in combination with particle tracking (Pollock, 2012). Mean velocity U and mean relative mass distribution $\langle \bar{m} \rangle$ are obtained by ensemble averaging.

Application to MADE The binary hydrofacies model was based on the granulometry of 214 samples taken from the 38 boreholes at *MADE* (Boggs et al., 1990), which is a data set completely independent from those of DPIL used by the *FOA* and *MIM-SCA* models. The parameters values pertinent to *MADE* were identified as: $p_1 = 0.145$, $p_2 = 0.855$, $K_1 = 190\,\mathrm{m/d}$, $K_2 = 1.49\,\mathrm{m/day}$, $L_{z,1} = 0.702\,\mathrm{m}$, $L_{z,2} = 4.15\,\mathrm{m}$. The low borehole density prevented reliable estimate of the transition probability in the horizon-

tal directions. Thus, isotropy is assumed in horizontal direction and the characteristic lengths were based on the integral scales identified by Rehfeldt et al. (1992) and assuming that the relationship $L_{1,z}/L_{1,h} = L_{2,z}/L_{1,h} = e$ apply, with e being the anisotropy ratio. Thus, horizontal length scales are obtained by dividing the vertical ones, by the estimate of $e = 0.0437$ (Rehfeldt et al., 1992), arriving at $L_{h,1} = 16.0\,m$, and $L_{h,2} = 94.8\,m$. In vertical direction the Markov model of transition probability fitted to the experimental one was used. As already mentioned above, the horizontal length scales values shall be regarded as estimates, affected by uncertainty. A check of the results obtained with different, smaller, values (not shown) led to similar plume mass distributions except for the long distance tail of minute mass. An ensemble of over 200 independent Monte Carlo realizations of the hydrofacies distribution were thus generated.

Flow was solved numerically with Modflow 2005 in a computational domain of $300 \times 100 \times 10\,\mathrm{m}^3$ with grid spacing of $1\,m$ in horizontal and $0.5\,m$ in vertical directions for each hydrofacies realization. Constant head boundary conditions were applied with a mean head gradient of $J = 0.003$. The adopted porosity value was $\theta = 0.31$. Advective transport was simulated by tracking 1000 particles, distributed according to the mass distribution measured at day 9 since the beginning of the tracer test and advected by the random velocity (in the absence of local dispersion) by means of the ModPath 6 package. The resulting ensemble mean velocity is $U = 0.079\,m/day$ with a standard deviation of 0.0046 m/d.

3.2.5 Binary Inclusions

Background Further simplification of the previous binary facies model is achieved by representing the high conductivity zones as rectangular inclusions submerged in the low conductivity matrix. Furthermore, for the high length to thickness ratio of the inclusions it was found that flow and transport can be modeled approximately as two-dimensional. We describe here briefly the application of the model to *MADE* presented in Zech et al. (2020), in which the stochastic conceptualization of the binary hydraulic conductivity took large scale deterministic information into account.

K-Structure The aquifer is modeled as binary random structure. The two possible conductivity values K_1 and K_2 represent areas of high and low conductivity, respectively. The spatial structure is given as non-overlapping conductivity blocks of length I and width I_v. Site specific topological features, are integrated as deterministic structures, such as layers or blocks of different average conductivity. The *MADE*-specific K-structure model is outlined below.

Flow and Transport Flow and transport is solved for every random K realization numerically making use of Darcy's Law and ADE solvers. Mean velocity U and mean relative mass distribution $\langle \bar{m} \rangle$ are obtained by ensemble averaging.

Applcation to MADE Zech et al. (2020) adopted the K-structure for *MADE* and its characterizing parameter values based on the inspection of the piezometric surface map of Boggs et al. (1992, Fig. 3), on two large scale pumping tests (Table 1) and on a few flow meter logs (Boggs et al., 1992). According to observations, the area near the source is dominated by low conductivity K_2 with inclusions of high K_1. The relative area of the inclusions is $p = 15\%$ determined from flow meter log analysis. Beyond a distance of 20 m downstream of the injection location the distribution is inverted: the bulk is dominated by the high conductivity K_1 with $p = 15\%$ inclusions of low K_2. The inclusions are of thickness $\ell_v = 0.5\,\mathrm{m}$ and length $\ell_h \in [5, 10, 20]\,\mathrm{m}$. The former was determined from flowmeter observations while the latter are subjected to parametric uncertainty. The range was determined from the ratio of thickness and observed anisotropy value. The random component of the model comprises of the locations of the three vertical inclusions of 0.5 m thickness, while length and horizontal position of inclusions are

fixed for every realization. Given the inclusion occurrence of $p = 15\%$, an aquifer thickness of 10 m and a thickness of 0.5 m, a total number of 3 inclusions per block are randomly placed in vertical position with equal probability. Altogether, an ensemble of 600 conductivity structures was created with random inclusion structures, with groups of 200 realizations of same length inclusion length ℓ_h of 5 m, 10 m or 20 m.

Flow and transport was calculated for every random K-structure solving the groundwater flow equation and subsequently the ADE with the FEM software OpenGeoSys in a 2D cross section of $220\,m \times 10\,m$. The boundary conditions were of constant head on the vertical boundaries defined by the selected head gradient $J = 0.003$. The initial condition for transport was imposed by injecting a solute discharge $Q_{in} = 1.15 \cdot 10^{-5}\,\mathrm{m}^3/\mathrm{s}$ during a period of $T_{in} = 48.5$ h in the injection well with a screen length of 0.6 m (Boggs et al., 1992). Porosity is $\theta = 0.32$, local dispersivity was $\alpha_L = 0.01$ m, not impacting the overall mass distribution. The resulting ensemble mean velocity was $U = 0.0254$ m/d with a standard deviation of 0.02 m/d.

3.2.6 Reactors

Background The reactor model conceptualizes subsurface solute transport as series of reactors which are linked to aquifer structure. The concept allows to model transport in a setting where tracer is injected into a low permeability zone, capturing strongly constrained downstream movement and skewed plume shapes. The concept was applied e.g. by Molin & Cvetkovic (2010).

K-Structure Hydraulic conductivity is conceptualized as log-normal spatial random function Y with continuous two-point correlation structure. The multi-Gaussian geostatistical parameters are those reported by Bohling et al. (2016) based on DPIL for the model application to *MADE* of same values as those adopted in the *First Order* and *MIMSCA* models (sections 3.2.1 and 3.2.2).

Flow Mean uniform flow velocity is calculated analytically based on Darcy's Law: $U = K_{\mathrm{eff}} \cdot J/\theta$. K_{eff} for *MADE* is derived analogously to the *MIMSCA* model from geostatistical parameters (Zarlenga et al., 2018), resulting in $U = 0.026$m/d.

Transport Transport is modelled analytically as series of flow reactors, each described by an exponential function $\exp(-t/\Delta\tau)$ of the mean turnover time $\Delta\tau$. While this model cannot be related directly to the permeability distribution, it is of interest to examine the outcome of a conceptually different model. The number of reactors is a function of the ratio $x/\Delta x$ of the transport domain size x and the velocity fluctuations length scale Δx. Each reactor has a mean turnover time of $\Delta\tau = \Delta x/U$ and thus a residence time pdf of $\exp(-tU/\Delta x)$.

The residence time pdf in the $x/\Delta x$ series of reactors is then a Gamma function:

$$f(t,x) = \frac{e^{-\frac{tU}{\Delta x}} t^{\frac{x}{\Delta x}-1} \left(\frac{U}{\Delta x}\right)^{x/\Delta x}}{\Gamma\left(\frac{x}{\Delta x}\right)} \tag{3}$$

The cumulative density function of residence time is obtained by integration as

$$F(t,x) = \int_0^t f(\theta,x)\,d\theta = 1 - \frac{\gamma\left(x/\Delta x, tU/\Delta x\right)}{\Gamma\left(x/\Delta x\right)} \tag{4}$$

where γ is the lower incomplete Gamma-function.

The spatial tracer distribution, as the tracer position pdf $p(x;t)$ [1/L] at time t follows as:

$$p(x,t) = -\frac{\partial F(t,x)}{\partial x} \tag{5}$$

$$= \frac{1}{\Delta x\,\Gamma\left(\frac{x}{\Delta x}\right)}\left[G^{3,0}_{2,3}\left(\frac{tU}{\Delta x}\middle|\begin{matrix}1,1\\0,0,\frac{x}{\Delta x}\end{matrix}\right) + \Gamma\left(\frac{x}{\Delta x},\frac{tU}{\Delta x}\right)\left(\log\left(\frac{tU}{\Delta x}\right) - \psi^{(0)}\left(\frac{x}{\Delta x}\right)\right)\right] \tag{6}$$

where G is the Meijer g-function, and ψ^0 is the Polygamma function. With unit tracer mass, we have $m(x,t) = p(x,t)$.

Note that in the limit $\Delta x \to 0$, the number of reactors tends to infinity $x/\Delta x \to \infty$, and we recover plug flow as $f(t,x) \to \delta(t - x/U)$.

Like in the *MIMSCA* model, the length parameter Δx, the integral scale of the velocity fluctuations, is assumed to be in the range of two to three log-conductivity horizontal correlation length I.

Application to MADE The value of $U = 0.026\ m/d$ is identical with the one used in the *FOA* or *MIMSCA* models and similarly $I = 9.1m$ is based on Bohling et al. (2016).

4 Prediction and Inter-comparison using MADE Data

4.1 Results Presentation

The visual presentation of results concerning the mass spatial distribution significantly influences the perception of model performance. Critical aspects are the display scale, data upscaling (aggregation) and normalization. We present longitudinal mass distributions $\langle \bar{m} \rangle$ at linear and logarithmic scales as well as in a cumulative form $\langle M \rangle$, to achieve a comprehensive display. The various display modes of the spatial mass distributions allow to interpret a few plume's specific features: (i) mass peak location and bulk behavior; (ii) the tails (forefront and trailing zones) and (iii) mass recovery. They are relevant to specific goals such as risk assessment and remediation.

In line with the *MADE* experimental results, we remind that $\langle \bar{m}(x,t) \rangle$ is aggregated over intervals of 10 m. We illustrate the effect by displaying the model outcomes at $T = 126$ days in both forms, the fine scale $\langle m(x,t) \rangle$ and the upscaled $\langle \bar{m}(x,t) \rangle$ (Fig. 3) as well as $\langle M \rangle$. All longitudinal mass distributions are normalized with respect to the injected mass such that the area beneath m or $\bar{m}$ is unity. For the *MADE* data this is only true for $t = T = 126$ days where mass recovery is around 99%.

Spatial moments are commonly used to quantify the comparison between different models and measurements. However, this is not appropriate because of the skewed shape of $\langle \bar{m} \rangle$ and the large impact of the uncertainty of the tail. Instead, we compare in Fig. 4 recovery locations at $T = 126$ days for 5%, 50%, and 95% as predicted by models relative to *MADE* values of $x = 0.7$, 8.6, 42.8 meters. The definition of the recovery location is for instance for $x_{95\%}$,the position for which 95% of the total mass is upstream of $x_{95\%}$, i.e. $\langle M \rangle = 0.95$.

Spatial moments are commonly used to quantify the comparison between different models and measurements. However, this is not appropriate because of the skewed shape of $\langle \bar{m} \rangle$ and in particular the large impact of the minute and uncertain mass fraction in the forefront tail, upon the second spatial moment (Fiori et al., 2017). Instead, we compare in Fig. 4 recovery locations at $T = 126$ days for 5%, 50%, and 95% as predicted by models relative to *MADE* values of $x = 0.7$, 8.6, 42.8 meters. The definition of the recovery location is for instance for $x_{95\%}$,the position for which 95% of the total mass is upstream of $x_{95\%}$, i.e. $\langle M \rangle = 0.95$.

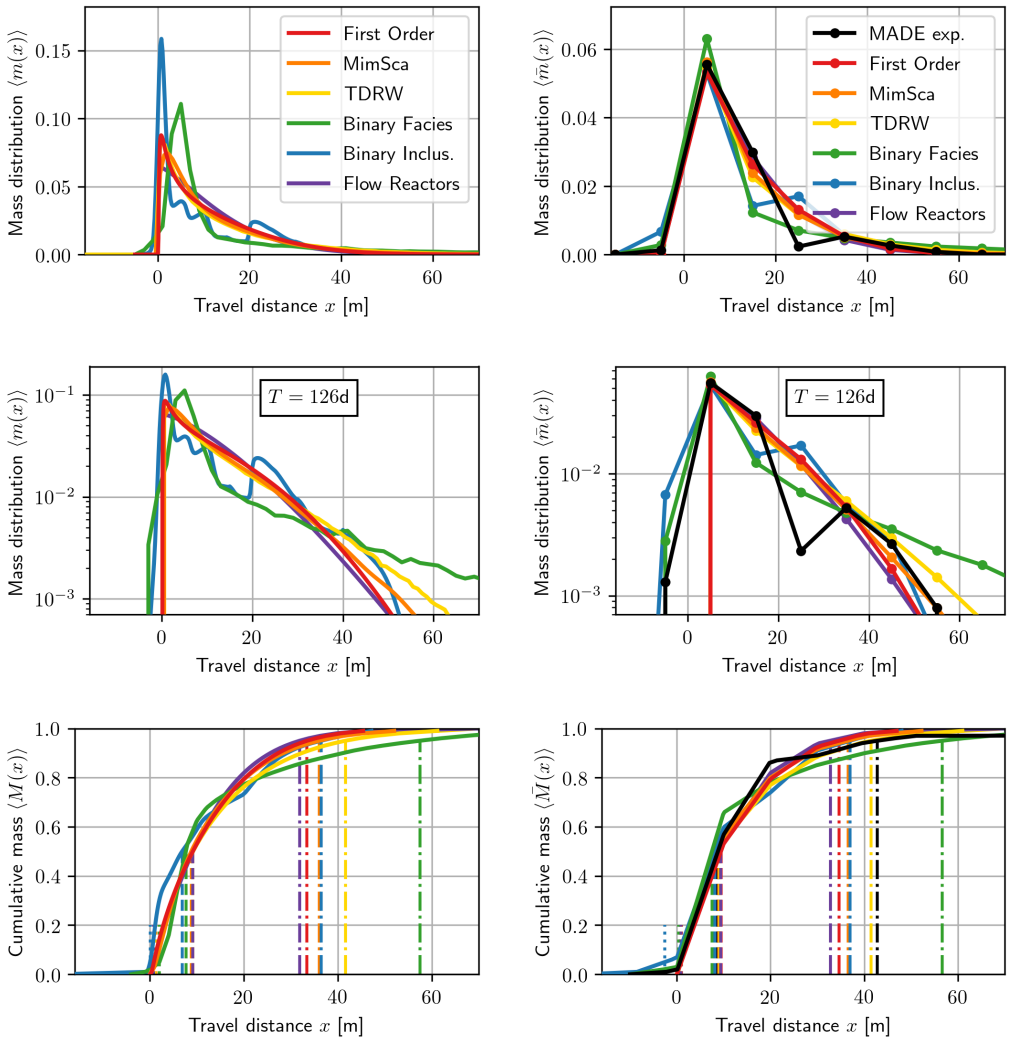

Figure 3. Longitudinal mass distribution for models at $T = 126\,\mathrm{d}$ in fine model resolution (left column) and upscaled (aggregated) form ($\Delta x = 10\,\mathrm{m}$, right column) against *MADE-1* experiment data at linear scale (1st row), log-scale (2nd row) and in cumulative mass (3rd row). Vertical lines in 3rd column indicate locations of 5% (dotted), 50% (dashed), and 95% (dashed dotted) recovered mass. Note that for the *Binary Facies* model the fine scale refers to a grid resolution of 2 meters.

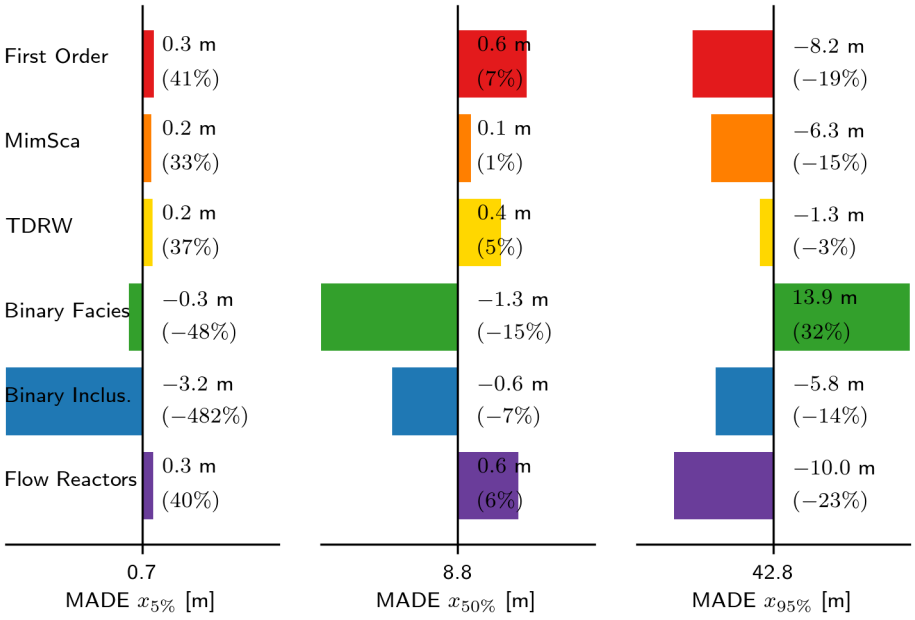

Figure 4. Model-experiment-comparison of recovery locations x for 5%, 50%, and 95% mass recovery (columns) at 126 days after injection where mass recovery was 99% in the experiment. *MADE* values at the x-axis [in m] and model values as absolute [in m] and relative [in %] difference in coloured bars and in numbers.

4.2 Comparison between Models Prediction and MADE Experiment

Fig. 3 displays the longitudinal mass distribution for all models and the *MADE* experimental data at $T = 126$ days after injection: $\langle m \rangle$ at model's fine resolution and $\langle \bar{m} \rangle$ aggregated over 10 m intervals, including *MADE*. Direct comparison is most revealing at that time since the experimental recovery rate is 99%.

The various models display some differences in their mass distribution $\langle m \rangle$ at fine scale. Particularly, the peak value is higher for the *Flow Reactors* by a factor of 2 than the other models. The *Binary Facies* model displays plume tailing downstream of the other models, with $x_{95\%} \cong 60m$ while for all the others models $30m \lesssim x_{95\%} \lesssim 40m$ (see Fig. 3).

The comparison between $\langle m \rangle$ and the upscaled $\langle \bar{m} \rangle$ in Fig. 3 reveals a few interesting features: upscaling reduces the peak values of $\langle m \rangle$ by a factor of around 2, the spreading zone is expanded, and the differences between models prediction are greatly reduced. In particular, the predicted $\langle \bar{m} \rangle$ agrees quite well with *MADE*, much better than $\langle m \rangle$, as far as visual inspection reveals. This is expectable though in the past models prediction at fine scale were compared with *MADE* (e.g. Harvey & Gorelick (2000); Dogan et al. (2014)). The upstream spread of the aggregated $\langle \bar{m} \rangle$ for *MADE* is partly an artifact of upscaling: it smears the upstream forced injected mass of the initial solute body over 10 meters. It could be erroneously interpreted as upstream dispersion.

The quantitative results in Fig. 4 on recovery locations relative to *MADE* strengthen the conclusions from the visual inspection. All models are in good agreement with *MADE* for the location $x_{50\%}$. We attribute that to the closeness of the mean velocity U of various models (see previous Section). The *Binary Facies* differs by 15% due to the differ-

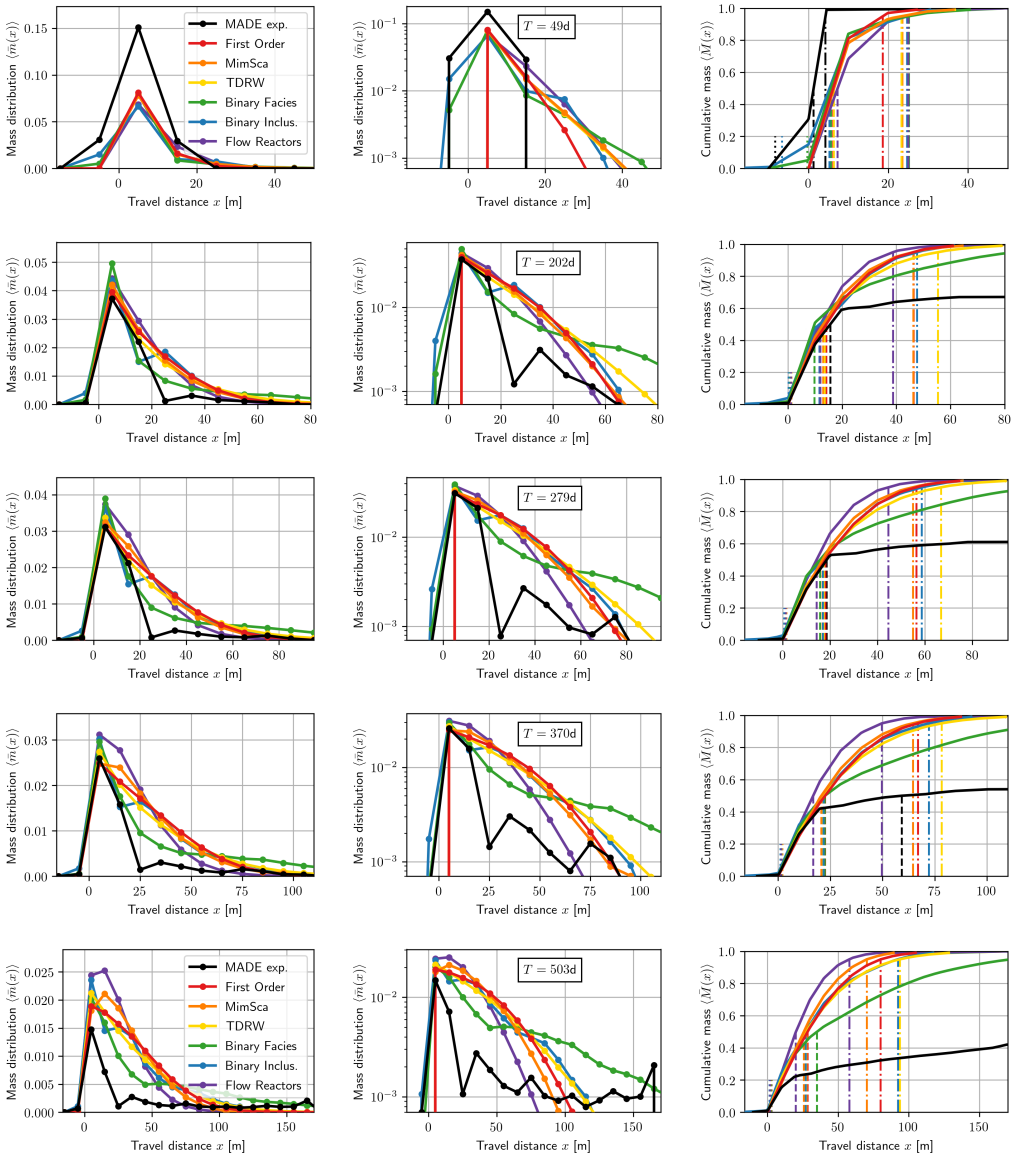

Figure 5. Longitudinal mass distribution for models and *MADE-1* experiment at 49, 202, 279, 370, and 503 days after injection at linear scale (1st column), log-scale (2nd column) and in cumulative form (3rd column) with recovery locations (Fig. 3). Observe the different recovery rates of $2.06, 0.68, 0.62, 0.54$, and 0.43, respectively.

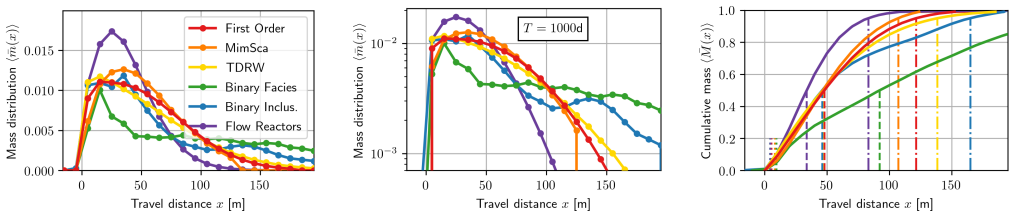

Figure 6. Longitudinal mass prediction of models at 1000 days at linear scale (1st column), log-scale (2nd column) and in cumulative form (3rd column) with recovery locations.

ence in the value of U. The agreement is still good for $x_{5\%}$ with some deviations for the *Binary Inclusion* model. Last, the models prediction relative to *MADE* of $x_{95\%}$, reflecting the "fast " moving solute, is more variable, but still within acceptable differences in practice.

Fig. 5 summarizes the model and *MADE* results of $\langle \bar{m} \rangle$ for all times for which *MADE* experimental data is available. The comparison at these times with *MADE* is more difficult than for $T = 126$ days because of the variable mass recovery, which is visible in Fig. 5 in the cumulative mass panel $\langle M \rangle$.

Our interpretation of the apparent "mass loss" for later times is the less dense sampling in the downstream zone as illustrated by Fig. 1 on one hand and the not-sampled solute quickly moving in high conductivity channels on the other hand, as already mentioned before. This is clearly visible in Fig. 5 displaying the larger predicted mass than the measured one downstream of the peak. Despite that, it is remarkable that for $T = 202, 270, 370$ days all models agree quite with both measured peak value and its distance from the injection zone. At the largest time $T = 503$ days the low mass recovery (43 %) makes the comparison between data and models prediction quite problematic. Still, the peak location and even the value are within acceptable differences in practice. As for inter-comparison of models prediction, inspection of the robust cumulative mass $\langle M \rangle$ at different times shows remarkable closeness except for *Binary Facies*. The latter overestimates the location $x_{\%}$ pertaining to fixed values of $\langle M \rangle > 0.4$. This enhanced tailing is attributed in part to the larger integral horizontal scale identified from granulometry analysis (Fig. 2) as compared to that resulting from DPIL, which was used by the most of the models. In addition, it may be related to channels of high conductivity present in some realizations of the binary K field. It is remarkable that for both $\langle \bar{m} \rangle$ and $\langle M \rangle$, the predictions by *FOA, MIMSCA* and *TDRW* are very close for all x (see discussion in Sect 5).

4.3 Prediction Beyond MADE Experiment

The important role of models is to provide prediction of future solute plumes development. In order to compare the outcome of the 6 different models considered in the present study, we have used them for the same *MADE* conditions, but at larger time than *T=503* days. Thus, the long term (at $T = 1000$ days) predicted plume mass spatial distribution is displayed in Fig. 6. All models agree in the peak travel distance as a consequence of similar flow velocities U. However, the differences between the peak value are more pronounced but still within a factor of two and even less for all models, except the *Reactors*, which predicts a higher peak and reduced tail. As for prediction of forefront tailing associated with fast moving solute, both *Binary Facies* and *Binary Inclusions* display longer tails with $80 \lesssim x_{95\%} \lesssim 140$ meters. Inspection of the cumulative

distribution reveals again that prediction of models except *Binary Facies* are within a relatively narrow distribution.

5 Discussion

5.1 Modelling

The main aim of the study is to compare the prediction of six different models, with *MADE* serving as a platform. However, based on conceptual similarity as well as prediction, the six models can be divided in three groups as follows: (i) *FOA* (First Order Approximation), *MIMSCA* (Multi Indicator and Self Consistent Approximation), and *TDRW* (Time Domain Random Walk); (ii) *BF* (Binary Facies) and *BI* (Binary Inclusions); and (iii) *Reactors*. Herein a discussion of the main results for each group.

(i) FOA, MIMSCA, *and* TDRW

For the three models K is modeled as a multi-Gaussian stationary random field, completely characterized by $K_{\rm G}$, σ^2_Y, I , I_v, the flow mean velocity being given by $U = K_{\rm eff}J/\theta$. They lead to approximate distributions of $\langle m\rangle$, $\langle \bar{m}\rangle$ and $\langle M\rangle$ as functions of x, t.

The three models differ in conceptualization and computational complexity. *FOA* is analytical, leading to an Inverse Gaussian $\langle m\rangle$ which satisfies an *ADE* with macrodispersivity derived analytically by *FOA*. *MIMSCA* is semi-analytical, based on summation of travel time through inclusions of random K. *TDRW* is semi-numerical, with the velocity field derived by *Monte Carlo* simulations while transport is based on an approximation of the *Lagrangian* velocity field.

One of our main result is that the solutions for $\langle \bar{m}\rangle$ and $\langle M\rangle$ by the three models are very close and in good agreement with the bulk of *MADE* experimental data. Thus they are are very robust and prediction depends primarily on U Fiori et al. (2017), as well as σ^2_Y and I and much less on models methodology.

(ii) BF *and* BI

The hydraulic conductivity heterogeneity is modeled by two values K_1, K_2 of volume fractions p_1 and $p_2 = 1-p_1$. Two length scales L_x, L_z characterize the K-facies, whose geometry has random elements. Flow and transport are solved numerically and repeatedly, by *Monte Carlo* simulations; besides the mean values U, $\langle \bar{m}\rangle$ and $\langle M\rangle$, the statistical moments of these parameters can be also obtained.

The two models differ in few respects: *BF* is three-dimensional; the random facies geometry is generated by transitional probability using the *TPROGS* code, which requires the knowledge of two more length scales for the second K-facies being different from the first. All the structural parameters are obtained from granulometry measurements. In contrast, the simpler *BI* model is two-dimensional and consists of identical rectangular inclusions of conductivity K_1 submerged in the K_2 matrix for specified deterministic regions. The inclusions lengths assume 3 different values of same probability, their elevation being random. The structural parameters K_1, K_2 and p_1, as well as the length scales, are derived from pumping tests and few flowmeter measurements.

The main results for these two models are as follows: the agreement with *MADE1* data is reasonable; while the characterization effort is less demanding than for the previous models, the numerical solutions and the *Monte Carlo* simulations of both flow and transport are quite involved, especially for *BF*.

The main conclusions are: the favorable comparison with *MADE1* is an additional proof of models robustness; the simplified structures and characterization are adapted

to the particular features of the *MADE* site for which two dominant zones could be delineated.

***(iii)* Reactors**

This model has a different conceptualization from the previous ones and it was motivated by its general use in engineering and convenience for reactive transport modelling. The model parameters are U, which is derived from the solution of flow via K_{eff}, and Δx, the velocity longitudinal correlation length which is related to I. The degree of heterogeneity quantified by σ_Y^2 is not included, instead the series of reactors aggregate the inherent dispersion of a flow reactor; thus the model is not a general candidate for modeling advective transport in a heterogeneous aquifer. Still, it was found of interest to compare the analytical solution for $\langle \bar{m} \rangle$ with *MADE* plume. The surprising result is that $\langle m \rangle$ and even more so $\langle \bar{m} \rangle$ agree reasonably well with *MADE*, though the predicted peak of $\langle \bar{m} \rangle$ is larger by a factor of 1.5 than prediction by other models for T =1000 days.

The finding strengthens the conclusion about the robustness of $\langle \bar{m} \rangle$ and $\langle M \rangle$ in predicting the measured *MADE* plume and its future development, with the predominant role of two parameters, the mean velocity U and correlation scale I; whether the reactors model can be used for prediction requires its further development and comparison with more cases.

5.2 Data Selection

The K distribution at the *MADE* site as inferred from different characterisation methods is summarized in Fig. 2: (i) DPIL measurements are a novel, affordable technique for shallow aquifers (Dietrich et al., 2008) by which the most comprehensive data set was obtained suitable for a geostatistical interpretation, including two-point statistics; (ii) Granulometry (or grain size analysis) is a standard method in hydrogeology that yields highly uncertain conductivity estimates (Vienken & Dietrich, 2011); (iii) flowmeter measurements and pumping tests are standard methods for hydrogeological characterisation, the main limitation being accuracy of low K values (Fig. 2).

The (semi-)analytical models *FOA*, *MIMSCA*, *TDRW*, and *Reactors* used DPIL observations to estimate the flow velocity and the plume spreading. The model *Binary Facies* (*BF*) used granulometry data and the *Binary Inclusions (BI*) model used pumping test estimates, information from head maps and a few flowmeter data. In essence, *BF* simplifies the facies approach applied by Bianchi and Zheng (2016) *MADE2* by considering 2 facies instead of 5, where the binary K values are inferred from granulometry. The *BI* approach simplifies further the 3D random structure by considering regular inclusions in two dimensions. Thus the semi-analytical models are relatively simple for computations but use a more extensive DPIL data set whereas *BI* and *BF* modelling approaches are heavier on computation but use more readily accessible data sets.

The derivation of the mean velocity U by the different models imply the use of estimates of the measured mean head gradient J and the effective porosity θ, which are approximate. The models differ primarily in the use of the K data. Still, the resulting estimates of the mean velocity U are relatively close as revealed by the values appearing in Sect. 3.2 (0.026m/d for *FOA,MIMSCA*, 0.019m/d for *TDRW*, 0.079m/d for *BF* and 0.025m/d for *BI*). Even the deviation for *BF* is within an acceptable range, various approximations notwithstanding. Thus, the estimates of U are quite robust, which explains the relative closeness of the predicted and measured locations of the peak of $\langle \bar{m} \rangle$ in Figures 3, 5, 6.

Similarly, the prediction of spreading as quantified by the $\langle \bar{m} \rangle$ and $\langle M \rangle$ distributions is quite robust, as already discussed above. An interesting finding which may somewhat explain the relative closeness of the distributions for different data characteriza-

tion methods is the magnitude of the *FOA* asymptotic longitudinal macrodispersivity $\alpha_L = \sigma_Y^2 I$ based on the different values of σ_Y^2 and I in Fig. 2. The resulting values of α_L are 53.7m, 54.1m and 49.6m for *DPIL, Flowmeter* and *Grain Size*, respectively.

Although above observations strictly apply to the *MADE* site only, they are nevertheless encouraging and motivate similar comparative analysis e.g., for less heterogeneous aquifers for which experimental data are available.

6 Summary and Conclusions

With a variety of hydraulic data available, *MADE* provides a unique opportunity for a comparative analysis of predictive modelling, from a wide range of (semi)-analytical models (*FOA, MIMSCA* and *TDRW*) that utilise extensive DPIL data for inferring geostatistical parameters, to numerical models (*BF* and *BI*) with relatively simple (binary) structures that utilise much less extensive data sets (granulometry and pumpoing tests+ flowmeter). The present paper takes advantage of these possibilities offered by *MADE*, and focuses on comparing predictions of the plume spreading by six different models. The models differ in theoretical formulations, in the conceptualization of aquifer structure, in the field data input, and in the computational effort. Common features of the models are: flow is steady, uniform in the mean and driven by a head gradient J; solute spreading is caused by aquifer conductivity heterogeneity; models rely on structural data and flow data with no calibration on transport observations i.e. the models are predictive; plume mass behavior is assumed ergodic, i.e. the mean relative mass distribution $\langle \bar{m} \rangle$ derived by the model is compared with the measured mass $\bar{m}$ at a few times T. Moreover, the apparent loss of mass of measured mass at *MADE1* for $T > 126$ days (attributed to limited sampling) is not taken into account by the models. Model comparison at $T = 1000$ days, i.e., beyond the period of measurements, is also included.

The main and encouraging result for practitioners is that all model prediction agree reasonably well with *MADE1* mass distributions and the same for the comparison at *T=1000* days. Thus, the measures of the solute plumes are robust and models are reliable as long as they are underlined by a few basic parameters: mean velocity U, a parameter reflecting log-conductivity variability and one taking horizontal correlations in conductivity into account. However, the reasonable agreement in model results is also related to the particular quantity under examination: the longitudinal mass distribution which is aggregated over spatial intervals is quite robust itself. If other measures are employed, such as local concentrations, results might differ.

To render the above conclusions of general validity, the study shall be extended by application to other cases than *MADE*. As a first step synthetic examples can be considered like formations of log-normal conductivity, with different connectivities as analyzed for instance by Fiori et al. (2017), or typical facies structures (e.g. Carle & Fogg (1996)). Similarly, one needs to test the hypothesis that a consistent comparison would have been obtained even for a less heterogeneous aquifer.

Acknowledgments

We thank Marco Bianchi and Boris Baeumer for their support during the development of the study. AF and AB acknowledge funding from the Italian Ministry of Education, University and Research (MIUR) in the frame of the Departments of Excellence Initiative 2018-2022 granted to Dept. of Engineering of Roma Tre University, and to the Dept. of Civil, Environmental and Mechanical Engineering of the University of Trento, respectively. MD acknowledges funding of the European Research Council (ERC) through the project MHetScale (contract number 617511), and the Spanish Research Agency (AEI) through the project HydroPore (contract number PID2019-106887GB-C31). Data on mod-

els and MADE observations can be found in the references. Scripts used in the paper are available upon request from the corresponding author.

References

Adams, E. E., & Gelhar, L. W. (1992). Field study of dipersion in a heterogeneous aquifer: 2. Spatial moments analysis. *Water Resour. Res.*, *28*(12), 3293–3307. doi: 10.1029/92WR01757

Barlebo, H. C., Hill, M. C., & Rosbjerg, D. (2004). Investigating the Macrodispersion Experiment (MADE) site in Columbus, Mississippi, using a three-dimensional inverse flow and transport model. *Water Resour. Res.*, *40*(4), W04211. doi: 10.1029/2002WR001935

Benson, D. A., Schumer, R., Meerschaert, M. M., & Wheatcraft, S. W. (2001). Fractional dispersion, Levy motion, and the MADE tracer tests. *Transp. Porous Media*, *42*(1-2), 211–240. doi: 10.1023/A:1006733002131

Berkowitz, B., & Scher, H. (2001). The role of probabilistic approaches to transport theory in heterogeneous media. *Transport in Porous Media*, *42*(1), 241–263. doi: 10.1023/A:1006785018970

Bianchi, M., & Zheng, C. (2016). A lithofacies approach for modeling non-Fickian solute transport in a heterogeneous alluvial aquifer. *Water Resour. Res.*, *52*, 552–565. doi: 10.1002/2015WR018186

Boggs, J. M., Schroeder, J., & Young, S. (1995). *Data to support model development for natural attenuation study* (Tech. Rep. No. WR28-2-520-197). Tennessee Valley Authority, Norris, Tennessee: TVA Engineering Laboratory.

Boggs, J. M., Young, S., Benton, D., & Chung, Y. (1990). *Hydrogeologic Characterization of the MADE Site* (Tech. Rep. No. EN-6915). Palo Alto, CA: EPRI.

Boggs, J. M., Young, S. C., Beard, L. M., Gelhar, L. W., Rehfeldt, K. R., & Adams, E. E. (1992). Field study of dispersion in a heterogeneous aquifer: 1. Overview and site description. *Water Resour. Res.*, *28*(12), 3281–3291. doi: 10.1029/92WR01756

Bohling, G. C., Liu, G., Dietrich, P., & Butler, J. J. (2016). Reassessing the MADE direct-push hydraulic conductivity data using a revised calibration procedure. *Water Resour. Res.*, *52*(11), 8970–8985. doi: 10.1002/2016WR019008

Bohling, G. C., Liu, G., Knobbe, S. J., Reboulet, E. C., Hyndman, D. W., Dietrich, P., & Butler, J. J. (2012). Geostatistical analysis of centimeter-scale hydraulic conductivity variations at the MADE site. *Water Resour. Res.*, *48*, W02525. doi: 10.1029/2011WR010791

Carle, S. F. (1999). *T-PROGS: Transition probability geostatistical software, version 2.1* (Tech. Rep.). University of California, Davis.

Carle, S. F., & Fogg, G. E. (1996). Transition probability-based indicator geostatistics. *Mathematical Geology*, *28*(4), 453–476. doi: 10.1007/BF02083656

Comolli, A., Hakoun, V., & Dentz, M. (2019). Mechanisms, Upscaling, and Prediction of Anomalous Dispersion in Heterogeneous Porous Media. *Water Resour. Res.*, *55*(10), 8197–8222. doi: 10.1029/2019WR024919

Cvetkovic, V., Fiori, A., & Dagan, G. (2014). Solute transport in aquifers of arbitrary variability: A time-domain random walk formulation. *Water Resour. Res.*, *50*(7), 5759–5773. doi: 10.1002/2014WR015449

Dagan, G. (1989). *Flow and transport on porous formations*. New York: Springer.

Dagan, G., & Cvetkovic, V. (1993). Spatial moments of a kinetically sorbing solute plume in a heterogeneous aquifer. *Water Resour. Res.*, *29*(12), 4053–4061. doi: 10.1029/93WR02299

Dagan, G., & Fiori, A. (2003). Time-dependent transport in heterogeneous formations of bimodal structures: 1. The model. *Water Resour. Res.*, *39*(5), 1112. doi: 10.1029/2002WR001396

Dentz, M., Comolli, A., Hakoun, V., & Hidalgo, J. (2020). Transport upscaling in highly heterogeneous aquifers and the prediction of tracer dispersion at the macrodispersion experiment (MADE) site. *Water Resour. Res.*.

Dentz, M., Kang, P. K., Comolli, A., Le Borgne, T., & Lester, D. R. (2016). Continuous time random walks for the evolution of Lagrangian velocities. *Phys. Rev. Fluids*, *1*(7), 074004. doi: 10.1103/PhysRevFluids.1.074004

Dietrich, P., Butler, J. J., & Faiss, K. (2008). A rapid method for hydraulic profiling in unconsolidated formations. *Ground Water*, *46*(2), 323–328. doi: 10.1111/j.1745-6584.2007.00377.x

Dogan, M., Van Dam, R. L., Liu, G., Meerschaert, M. M., Butler, J. J., Bohling, G. C., ... Hyndman, D. W. (2014). Predicting flow and transport in highly heterogeneous alluvial aquifers. *Geophys. Res. Lett.*, *41*, 7560–7565. doi: 10.1002/2014GL061800

Feehley, C. E., Zheng, C., & Molz, F. J. (2000). A dual-domain mass transfer approach for modeling solute transport in heterogeneous aquifers: Application to the Macrodispersion Experiment (MADE) site. *Water Resour. Res.*, *36*(9), 2501–2515. doi: 10.1029/2000WR900148

Fetter, C. W., Boving, T., & Kreamer, D. (2018). *Contaminant hydrogeology* (3rd ed.). Long Grove, Ill: Waveland Pr Inc.

Fiori, A. (2014). Channeling, channel density and mass recovery in aquifer transport, with application to the MADE experiment. *Water Resour. Res.*, *50*(12), 9148–9161. doi: 10.1002/2014WR015950

Fiori, A., Dagan, G., Jankovic, I., & Zarlenga, A. (2013). The plume spreading in the MADE transport experiment: Could it be predicted by stochastic models? *Water Resour. Res.*, *49*(5), 2497–2507. doi: 10.1002/wrcr.20128

Fiori, A., Jankovic, I., & Dagan, G. (2003). Flow and transport through two-dimensional isotropic media of binary conductivity distribution. Part 1: NUMERICAL methodology and semi-analytical solutions. *Stochastic Environmental Research and Risk Assessment*, *17*(6), 370–383. doi: 10.1007/s00477-003-0166-0

Fiori, A., Jankovic, I., & Dagan, G. (2006). Modeling flow and transport in highly heterogeneous three-dimensional aquifers: Ergodicity, Gaussianity, and anomalous behavior — 2. Approximate semianalytical solution. *Water Resour. Res.*, *42*(6), W06D13. doi: 10.1029/2005WR004752

Fiori, A., Zarlenga, A., Bellin, A., Cvetkovic, V., & Dagan, G. (2019). Groundwater contaminant transport: Prediction under uncertainty, with application to the MADE transport experiment. *Front. Environ. Sci.*, *7*. doi: 10.3389/fenvs.2019.00079

Fiori, A., Zarlenga, A., Jankovic, I., & Dagan, G. (2017). Solute transport in aquifers: The comeback of the advection dispersion equation and the First Order Approximation. *Adv. Water Resour.*, *110*, 349–359. doi: 10.1016/j.advwatres.2017.10.025

Gelhar, L. (1993). *Stochastic subsurface hydrology.* N. Y.: Prentice Hall, Englewood Cliffs.

Gomez-Hernandez, J., Butler, J. J., Fiori, A., Bolster, D., Cvetkovic, V., Dagan, G., & Hyndman, D. (2017). Introduction to special section on modeling highly heterogeneous aquifers: Lessons learned in the last 30 years from the MADE experiments and others. *Water Resour. Res.*, *53*(4), 2581–2584. doi: 10.1002/2017WR020774

Hakoun, V., Comolli, A., & Dentz, M. (2019). Upscaling and prediction of Lagrangian velocity dynamics in heterogeneous porous media. *Water Resour. Res.*, *55*(5), 3976–3996. doi: 10.1029/2018WR023810

Harvey, C. F., & Gorelick, S. M. (2000). Rate-limited mass transfer or macrodispersion: Which dominates plume evolution at the Macrodispersion Experiment (MADE) site? *Water Resour. Res.*, *36*(3), 637–650. doi: 10.1029/

1999WR900247

Hess, K., Wolf, S., & Celia, M. (1992). Large-scale natural gradient tracer test in sand and gravel, Cape-Cod, Massachusetts .3. Hydraulic conductivity variability and calculated macrodispersivities. *Water Resour. Res.*, *28*(8), 2011–2027. doi: 10.1029/92WR00668

Jankovic, I., Fiori, A., & Dagan, G. (2003). Flow and transport in highly heterogeneous formations: 3. Numerical simulations and comparison with theoretical results. *Water Resour. Res.*, *39*(9), 1270. doi: 10.1029/2002WR001721

Jankovic, I., Maghrebi, M., Fiori, A., & Dagan, G. (2017). When good statistical models of aquifer heterogeneity go right: The impact of aquifer permeability structures on 3d flow and transport. *Adv. Water Resour.*, *100*, 199–211. doi: 10.1016/j.advwatres.2016.10.024

Kreft, A., & Zuber, A. (1978). Physical meaning of dispersion-equation and its solutions for different initial and boundary-conditions. *Chem. Eng. Sci.*, *33*(11), 1471–1480. doi: 10.1016/0009-2509(78)85196-3

Molin, S., & Cvetkovic, V. (2010). Microbial risk assessment in heterogeneous aquifers: 1. Pathogen transport. *Water Resour. Res.*, *46*(5). doi: 10.1029/2009WR008036

Noetinger, B., Roubinet, D., Russian, A., Le Borgne, T., Delay, F., Dentz, M., ... Gouze, P. (2016). Random walk methods for modeling hydrodynamic transport in porous and fractured media from pore to reservoir scale. *Transp Porous Med*, *115*(2), 345–385. doi: 10.1007/s11242-016-0693-z

Pollock, D. W. (2012). *User guide for modpath version 6 - a particle-tracking model for modflow* (Tech. Rep. No. 6-A41). Reston, VA: U.S. Geological Survey. doi: 10.3133/tm6A41

Rehfeldt, K. R., Boggs, J. M., & Gelhar, L. W. (1992). Field study of dispersion in a heterogeneous aquifer: 3. Geostatistical analysis of hydraulic conductivity. *Water Resour. Res.*, *28*(12), 3309–3324. doi: 10.1029/92WR01758

Rehfeldt, K. R., Hufschmied, P., Gelhar, L. W., & Schaefer, M. (1989). *Measuring hydraulic conductivity with the borehole flowmeter* (Tech. Rep. No. EN-6511). Palo Alto, CA: EPRI.

Riva, M., Guadagnini, L., & Guadagnini, A. (2010). Effects of uncertainty of lithofacies, conductivity and porosity distributions on stochastic interpretations of a field scale tracer test. *Stochastic Environmental Research and Risk Assessment*, *24*(7), 955–970. doi: 10.1007/s00477-010-0399-7

Rubin, Y. (2003). *Applied stochastic hydrogeology.* New York: Oxford Univ. Press.

Salamon, P., Fernàndez-Garcia, D., & Gòmez-Hernández, J. J. (2007). Modeling tracer transport at the MADE site: The importance of heterogeneity. *Water Resour. Res.*, *43*(8), W08404. doi: 10.1029/2006WR005522

Sudicky, E. (1986). A natural gradient experiment on solute transport in a sand aquifer: Spatial variability of hydraulic conductivity and its role in the dispersion process. *Water Resour. Res.*, *22*, 2069–2082.

Suribhatla, R., Jankovic, I., Fiori, A., Zarlenga, A., & Dagan, G. (2011). Effective conductivity of an anisotropic heterogeneous medium of random conductivity distribution. *Multiscale Model. Simul.*, *9*(3), 933–954. doi: 10.1137/100805662

Vienken, T., & Dietrich, P. (2011). Field evaluation of methods for determining hydraulic conductivity from grain size data. *J. Hydrol.*, *400*(1-2), 58–71. doi: 10.1016/j.jhydrol.2011.01.022

Zarlenga, A., Jankovic, I., Fiori, A., & Dagan, G. (2018). Effective hydraulic conductivity of three-dimensional heterogeneous formations of lognormal permeability distribution: The impact of connectivity. *Water Resour. Res.*, *54*(3), 2480–2486. doi: 10.1002/2017WR022141

Zech, A., Attinger, S., Cvetkovic, V., Dagan, G., Dietrich, P., Fiori, A., ... Teutsch, G. (2015). Is unique scaling of aquifer macrodispersivity supported by field data?

Water Resources Research, *51*(9), 7662–7679. doi: 10.1002/2015WR017220

Zech, A., Dietrich, P., Attinger, S., & Teutsch, G. (2020). A field evidence model: How to predict transport in a heterogeneous aquifers at low investigation level? *Hydrology and Earth System Sciences Discussions*, 1–21. doi: https://doi.org/10.5194/hess-2020-30

Zheng, C., Bianchi, M., & Gorelick, S. M. (2011). Lessons learned from 25 years of research at the MADE site. *Ground Water*, *49*(5), 649–662. doi: 10.1111/j.1745-6584.2010.00753.x